IDEALIZED MOIST RAYLEIGH-BÉNARD CONVECTION WITH PIECEWISE LINEAR EQUATION OF STATE[*]

OLIVIER PAULUIS[†] AND JÖRG SCHUMACHER[‡]

Dedicated to the sixtieth birthday of Professor Andrew Majda

Abstract. An idealized framework to study the impacts of phase transitions on atmospheric dynamics is described. Condensation of water vapor releases a significant amount of latent heat, which directly affects the atmospheric temperature and density. Here, phase transitions are treated by assuming that air parcels are in local thermodynamic equilibrium, which implies that condensed water can only be present when the air parcel is saturated. This reduces the number of variables necessary to describe the thermodynamic state of moist air to three. It also introduces a discontinuity in the partial derivatives of the equation of state. A simplified version of the equation of state is obtained by a separate linearization for saturated and unsaturated parcels. When this equation of state is implemented in a Boussinesq system, the buoyancy can be expressed as a piecewise linear function of two prognostic thermodynamic variables, D and M, and height z. Numerical experiments on the nonlinear evolution of the convection and the impact of latent heat release on the buoyant flux are presented.

Key words. Convection, atmospheric dynamics, clouds.

AMS subject classifications. 76F35, 76F65, 76R10, 86A15.

1. Introduction

Water vapor accounts for less than 2 percent of the mass of the atmosphere, but plays a fundamental role in many atmospheric phenomena, ranging from clouds, thunderstorms, and hurricanes to the global circulation. This is due to the fact that, of all atmospheric gases, only water is present in all three phases within the Earth's atmosphere. Phase transitions — condensation of water vapor in cloud droplets or ice crystals, freezing and evaporation of liquid water, and melting and sublimation of ice — are associated with a conversion between latent energy and sensible (thermal) energy. The amount of energy involved with the hydrological cycle is considerable: when averaged globally, condensation is associated with a net release of approximately $75W/m^2$ in the atmosphere. This energy is initially injected into the atmosphere through evaporation at the Earth's surface and is transported by atmospheric motions to the regions where condensation takes place. Its full impact on temperature and density is only felt when water vapor condenses so that latent heat of vaporization is converted into the thermal energy of the air molecules.

Most of the time, water vapor condenses as a result of atmospheric motions. When an air parcel rises, it expands adiabatically and its temperature and saturation vapor pressure drop. During its ascent, a parcel might become saturated, in which case, water condenses and a cloud is formed. Most clouds in the atmosphere occur within ascending motions on scales ranging from a few hundred meters for cumulus clouds, to a few thousand kilometers in the case of the weather systems that dominate the midlatitudes. Atmospheric circulations play a critical role not only in transporting water vapor, but also in determining when and where condensation occurs.

Condensation is not simply a response to atmospheric motions, but has a direct impact on the dynamics itself. Indeed, when water condenses, it releases latent heat and warms the air parcel, making it lighter. The condensation of $1g$ of water is enough to raise the temperature of $1kg$ of air by $2.5K$. Water vapor concentration in the atmosphere can exceed $20g$ per kg. If all this latent heat were converted into thermal energy, the temperature of an air parcel would increase by $50K$ and its density would decrease by approximately 15%. These dual feedbacks - atmospheric motions controlling condensation and latent heat release affecting air density - are the core of a complex interplay between dynamics and thermodynamics.

Moist dynamics aims at understanding the impacts of phase transitions on atmospheric flows. This includes a wide range of issues, such as microphysical processes involving cloud drops and ice crystals, turbulent mixing between cloudy air and its environment, interactions between different clouds, organization of convection on the meso-scale, various weather systems such as hurricanes or midlatitude storms, and the global distribution of precipitation. This is an area of active research, with direct implications for our understanding of the climate system. In its Fourth Assessment Report, the Intergovernmental Panel on Climate Change assesses that "cloud feedbacks remain the largest source of uncertainty" in predicting future climate change [30].

This situation might be changing due to a combination of improvements in our ability to simulate cloud systems and a renewed theoretical focus on moist dynamics. A new generation of high-resolution Cloud Systems Resolving Models (CSRMs) offers a new and powerful tool to address the long-standing issue of how convective systems interact with their environment. General Circulation Models (GCMs) have a horizontal resolution on the order of $100\ km$, which is insufficient to resolve convective motions. As a result, convection and the various associated clouds must be parameterized in GCMs through some semi-empirical closure. In contrast, CSRMs have a horizontal resolution of the order of 1–$2\ km$, sufficient to explicitly simulate the processes associated with the organization of convection. These models have been shown to reproduce the observed behavior of convection much more accurately than the parameterizations used in GCMs [27]. The development of CSRMs was initially driven in the 1980s by studies of deep convection over limited areas [13, 16]. However, a continuous increase in computing resources has greatly expanded their possible applications, both in terms of domain size and length of simulations [11, 33, 10]. A global CSRM should be available for climate simulations within the next decade, but it is already possible today to take advantage of CSRMs to investigate the interactions between convection and the large-scale circulation.

In parallel with these new modeling capabilities, significant progress has been made on a wide range of theoretical issues related to the role of water vapor in atmospheric circulation, such as midlatitude storms, the energetics of the atmosphere, turbulent mixing in cloud dynamics, and large-scale dynamics in the tropics. Cooperation between mathematicians and atmospheric physicists has been particularly fruitful in developing new tools and techniques, such as a systematic methodology to derive the reduced dynamics governing different scales of motion, as well as a formal derivation of the terms leading to the multi-scale interactions [21, 20, 19]. In [2], this novel approach has already been successfully applied to stress the role of scale interactions in the Madden-Julian Oscillation [17, 18], the dominant mode of variability on the intra-seasonal scale in the tropical atmosphere. Water vapor and phase transitions can lead to novel dynamical behavior, such as the so-called precipitation front

[9, 32, 26]. The precipitation front theory demonstrates that, in an idealized model, the interface between the precipitating and non-precipitating regions act as a dynamical shock: solutions exhibit a discontinuity in the vertical velocity and precipitation fields, and move at a speed distinct from the characteristics of the flow [9]. As models become increasingly complex, there is also an increasing need for new theoretical framework that can shed light on how dynamics and thermodynamics interact in a moist atmosphere.

This paper introduces an idealized framework to study the effects of phase transition on atmospheric dynamics. Our hope here is that the framework could lead to new mathematical and physical insights on the effects of phase transition on atmospheric motions on the cloud scale from a few hundred meters to a few hundred kilometers, corresponding to a typical CSRM simulation. The framework discussed here favors mathematical simplicity over physical accuracy. It was originally introduced by Bretherton [5, 6], but has not been systematically studied since. In section 2, we first review the thermodynamic properties of moist air, and show that, under the assumptions of thermodynamic equilibrium, phase transitions introduce a discontinuity in the partial derivatives of the equation of state. Section 3 discusses an idealized system for a 'moist' fluid whose equation of state is piecewise linear. Its primary advantage is that it provides the simplest fluid dynamical framework in which the impacts of phase transition can be explicitly investigated. Finally, in section 4, we introduce a moist analog to the Rayleigh-Bénard convection problem, and discuss some of its properties by means of numerical simulations.

2. The equation of state for moist air

In thermodynamics, the concept of state variable refers to any quantitative property that depends on the state of the system only, e.g. its pressure, temperature, volume, chemical composition or energy content. Not all combinations of state variables are physically realisable. In general, the state of a fluid can be uniquely defined by a combination of a finite number of selected variables. For example, the state of an ideal gas is uniquely determined by its temperature T and pressure p. Once these specific state variables are known, all other state variables can be derived. The equation of state refers to the relationship between different state variables that restrict the range of possible combinations to those that are physically realizable. In practice, this is used to infer the value of certain state variables from the knowledge of others. One of the better-known examples is the equation of state for an ideal gas which relates the specific volume α of a gas to its temperature T and pressure p by

$$\alpha = \frac{RT}{p}, \qquad (2.1)$$

with R being the specific gas constant.

For most practical applications, moist air can be treated as a mixture of dry air, water vapor, and condensed water. In meteorology, 'dry air' refers to the mixture of atmospheric gases - mostly oxygen, nitrogen, argon and carbon dioxide - with the exclusion of water vapor and condensed water. The composition of dry air is remarkably uniform through the entire atmosphere, except for stratospheric ozone. The state of a parcel of moist air can be obtained from the knowledge of four of its state variables, for example the pressure p, temperature T, water vapor concentration q_v and condensed water concentration q_l. This means that any other thermodynamic quantities such as enthalpy or specific volume can be written as a function of these four variables $F = F(T, q_v, q_l, p)$.

Not all combinations of the four state variables can be observed in the atmosphere. This is due to the fact that water can spontaneously change phases. Evaporation and condensation act to restore the thermodynamic equilibrium between water vapor and liquid water. The saturation water vapor pressure $e_s(T)$ is the partial pressure of the water vapor in thermodynamic equilibrium with liquid water at temperature T. If too much water vapor is present, in the sense that the partial pressure of water vapor e is larger than the saturation value $e > e_s(T)$, some vapor will condense onto cloud droplets or water crystals. Conversely, when the water vapor pressure is less than the saturation vapor $e < e_s(T)$, condensed water will evaporate. We refer to unsaturated air, saturated and supersaturated air as air in which the water vapor pressure is respectively less than, equal to or larger than the saturation value. The degree of saturation can be measured through the relative humidity $\mathcal{H}$ defined as the ratio between the partial pressure of water vapor to its saturation value $\mathcal{H} = e/e_s(T)$ so that saturated air corresponds to $\mathcal{H} = 1$.

The adjustment to thermodynamic equilibrium is very fast. Observations indicate that there is very little supersaturation in clouds, with the relative humidity remaining less than 101%, and unsaturated air is only present in the absence of condensed water. There are two notable exceptions: the presence of super-cooled water at temperature as low as $-40^0 C$, and precipitation falling through unsaturated air without re-evaporating instantly. Outside these two special cases, atmospheric air parcels can be treated as being in local thermodynamic equilibrium, i.e., the conditions for thermodynamic equilibrium apply to each parcel separately. For moist air, this assumption implies that air parcels can be subdivided into two categories: unsaturated parcels in which only water vapor is present, and saturated parcels in which the partial pressure of water vapor is equal to its saturation value.

The requirement that air parcels are in thermodynamic equilibrium introduces an additional constraint on the state of moist air. It reduces the number of variables required to describe the state of moist air to three. Here, we introduce a new state variable, the total water content $q_T = q_v + q_l$. Once the total water content is known as well as two other state variables such as pressure and temperature, it is possible to use the thermodynamic equilibrium assumption to determine how the total water content is split between the vapor and condensed phase. The concentration of water vapor at saturation is the amount of water that would be present in a saturated parcel, and is given by

$$q_s(T, q_T, p) = \frac{R_v}{R_d} \frac{e_s(T)}{p - e_s(T)} (1 + q_T), \tag{2.2}$$

where R_v and R_d are the ideal gas constants for water vapor and dry air. If the total water content q_T is smaller than the saturated value q_s, then the parcel is unsaturated and all the water is in the gas phase. Otherwise, the parcel is saturated with the condensed and gas phases in thermodynamic equilibrium and it follows that

$$q_v = \begin{cases} q_T & \text{for } q_T \le q_s(T, q_T, p) \\ q_s(T, q_T, p) & \text{for } q_T > q_s(T, q_T, p) \end{cases} \tag{2.3a}$$

$$q_l = \begin{cases} 0 & \text{for } q_T \le q_s(T, q_T, p) \\ q_T - q_s(T, q_T, p) & \text{for } q_T > q_s(T, q_T, p). \end{cases} \tag{2.3b}$$

Equations (2.3a)–(2.3b) exhibit a key mathematical property of the equation of state of moist air: the fact that its partial derivatives are discontinuous at saturation.

Indeed, the partial derivative of the water vapor concentration with respect to the total water concentration is given by

$$\left(\frac{\partial q_v}{\partial q_T}\right)_{p,T} = \begin{cases} 1 & \text{for } q_T < q_s(T,q_T,p) \\ \frac{q_s(T,q_T,p)}{1+q_T} & \text{for } q_T > q_s(T,q_T,p). \end{cases} \tag{2.4}$$

Such a discontinuity in the partial derivative is not limited to water vapor concentration, but extends to relationships between a wide range of physical properties, such as temperature, specific volume, internal energy, or entropy. This property of the equation of state is the mathematical translation of the fact that saturated and unsaturated air behave as two very different fluids.

This can be illustrated by one of its repercussions in tropical meteorology. The lapse rate is defined as negative of the derivative of the temperature with height, $\Gamma = -\partial T/\partial z$. For a typical tropical sounding, it is roughly $0.01 K m^{-1}$ near the surface, but decreases abruptly to a value of the order of $0.004 K m^{-1}$ above the cloud base, usually at about $500\ m$ above the ground. In [35] it has been shown that the tropical lapse rate is close to that of a parcel raised adiabatically from the surface, i.e., $\Gamma = -\partial p/\partial z (\partial T/\partial p)_{S,q_T}$, with p being the parcel pressure and S the entropy per unit mass of moist air. When a parcel is lifted adiabatically, its pressure drops, its volume increases, and, as a result of this expansion, its temperature drops. For an unsaturated parcel, such cooling has no effect on the water vapor concentration. In contrast, once a parcel is saturated, any cooling also reduces the saturation vapor pressure. This forces some water vapor to condense, and the latent heat released by this condensation compensates for part of the cooling. Since condensation starts as soon as the parcel becomes saturated, the lapse rate of an adiabatic ascent drops sharply when the parcel becomes saturated at the cloud base.

As discussed above, the state of a parcel of moist air in local thermodynamic equilibrium is uniquely determined by the combinations of any three independent state variables. The temperature T might be a natural choice for describing a thermodynamic system at rest. Here, we will rather use the entropy per unit mass of moist air S, defined as (see [8] for a derivation)

$$S = [(1-q_T)C_{pd} + q_T C_l]\ln\frac{T}{T_o} + (1-q_T)R_d\ln\frac{p_d}{p_o} + q_v\frac{L_v}{T} - q_v R_v\ln\mathcal{H}. \tag{2.5}$$

Here, C_{pd} and C_l are the specific heat capacities at constant pressure of dry air and liquid water, p_d is the partial pressure of dry air, L_v is the latent heat of vaporization, and $\mathcal{H}$ is the relative humidity. The quantities T_o and p_o are arbitrary values for the reference temperature and pressure. One advantage of using entropy over temperature lies in that it can often be assumed that atmospheric motions are both adiabatic and reversible, which implies that the entropy of a parcel is conserved.

All thermodynamic properties of moist air can be expressed as a function of its entropy S, pressure p, and total water content q_T, i.e., $F = F(S,q_T,p)$. In most cases, the function F can be quite complex, and is rarely analytic. In practice, the properties of moist air are computed by deriving relations for the temperature $T = T(S,q_T,p)$, water vapor content $q_v = q_v(S,q_T,p)$, and liquid water content $q_l = q_l(S,q_T,p)$. The most common procedure is to first compute the temperature T by inverting the expression (2.5) assuming that the parcel is unsaturated $q_v = q_T$. One must then check whether the partial pressure of the water vapor e is smaller than the saturation pressure $e_s(T)$. If this is the case, the parcel is indeed unsaturated and the calculations are

over. Otherwise, the parcel is saturated, and one must recompute the temperature by inverting (2.5) for a saturated parcel with $q_v = q_s(T, q_T, p)$. Once the temperature and water vapor concentration have been computed, it is straightforward to retrieve other thermodynamic properties. While this procedure can be cumbersome, it is routinely performed in atmospheric models, and does not present any technical difficulties. Figure 2.1 shows the value of the temperature T and specific volume α as a function of the joint distribution of the entropy and total water content at a pressure of $900mb$. The dashed line marks the separation between saturated and unsaturated states, with the saturated parcels on the high-q_T portion of graph. The isotherms and isochores (lines of constant α) form an angle where they intercept the separation line, which is evidence of the discontinuity in the partial derivatives of T and α.
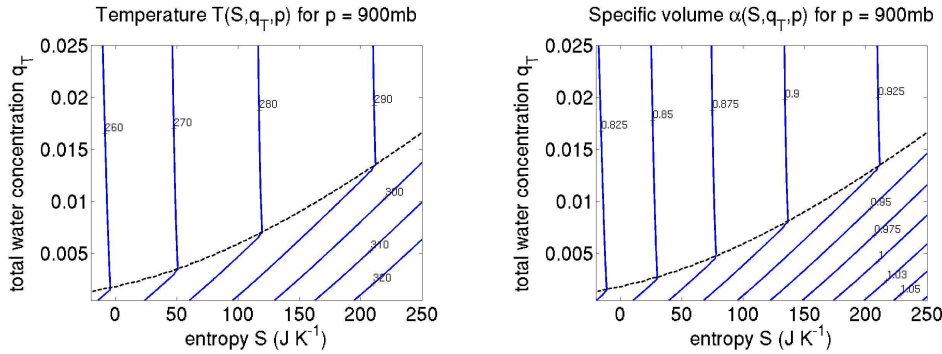

FIG. 2.1. *Temperature T (left panel) and specific volume α (right panel) as function of the parcel entropy S and total water concentration q_T for a constant pressure $p = 900mb$. Contour intervals are $10K$ for the temperature and $0.025 m^3 kg^{-1}$ for the specific volume. The dashed line indicates the boundary between saturated and unsaturated parcels, with the saturated parcels above the line.*

3. Boussinesq system with a piecewise linear equation of state

3.1. Boussinesq equations for a moist atmosphere. The Boussinesq equations [22, 4, 31] have been widely used to study atmospheric motions.[1] The derivation of the Boussinesq approximation for a compressible fluid requires definition of a reference profile with a uniform entropy S_{ref} and total water content $q_{T,ref}$. This reference state is hydrostatic, which implies that the reference pressure p_{ref} is obtained by integrating the hydrostatic balance $\partial p_{ref}/\partial z = -\rho(S_{ref}, q_{T,ref}, p_{ref}(z))g$. The governing equations are obtained by expanding the momentum and continuity equations under the assumption that the pressure and density are a small perturbation from these reference profiles

$$\frac{d\mathbf{u}}{dt} = -\nabla p' + B\mathbf{k} + \nu \nabla^2 \mathbf{u}, \tag{3.1}$$

$$\nabla \cdot \mathbf{u} = 0. \tag{3.2}$$

Here, $\mathbf{u}$ is the three-dimensional velocity, p' is pressure perturbation normalized by the density of the reference profile, B is the buoyancy, ν is the kinematic viscosity,

---

[1]The anelastic approximation [23, 16, 7, 1] is an alternative to the Boussinesq approximation that allows for vertical variation of density in the reference profile. It is commonly used to study atmospheric circulations, in particular deep convection. For the purpose of this paper, the Boussinesq approximation offers a slightly simpler framework.

and $\mathbf{k}$ denotes the unit vector in z direction. The time derivative d/dt in (3.1) is the so-called substantial (or material) derivative.

The buoyancy is defined in terms of the difference between the specific volume α of the parcel density and that of the environment

$$B(S,q_T,z) = g\frac{\alpha(S,q_T,p_{ref}(z)) - \alpha_{ref}(z)}{\alpha_{ref}(z)}. \tag{3.3}$$

Note that the specific volume is evaluated at the reference pressure $p_{ref}(z)$ rather than the total pressure $p_{ref}(z) + p'(z)$ in equation (3.3). Quantity g is the gravity acceleration.

Equations (3.1)–(3.3) are however incomplete as one needs to predict the evolution of the density field. In the case of moist air, this can be done by providing two prognostics for two state variables. Here, we use the entropy S and total water content q_T. Their dynamics are given by:

$$\frac{dS}{dt} = \dot{S} + \kappa\nabla^2 S \tag{3.4}$$

$$\frac{dq_T}{dt} = \dot{q_T} + \kappa\nabla^2 q_T, \tag{3.5}$$

with κ being the diffusivity, and $\dot{S}$ and $\dot{q_T}$ being the production rates of entropy and water in the atmosphere. While there are other alternatives, the choice of entropy and total water content for the prognostic variables has the advantage that both are conserved for reversible, adiabatic motions, i.e $dS/dt = dq_T/dt = 0$.

The system of equations (3.1)–(3.5) can be solved once the boundary conditions are set and the internal sources of entropy $\dot{S}$ and water $\dot{q_T}$ are determined. It differs from the traditional Boussinesq system for a single component fluid in that the buoyancy is determined by the equation of state for moist air, and depends on the two prognostic variables S and q_T and the height z. Reference [25] discusses in greater detail the use of a nonlinear equation of state in the anelastic and Boussinesq approximation and shows that such a system is consistent with both the first and second laws of thermodynamics. The approach here takes advantage of the conservation law for the entropy S and total water q_T to implicitly include phase transition through the equation of state, rather than explicitly computing the latent heat release by condensation as in the early discussions of moist convection [3, 14, 15],

3.2. Piecewise linear equation of state.   The equation of state for moist air is highly nonlinear. In addition to the discontinuity in the partial derivatives at saturation, other nonlinearities arise from the expression for entropy, from the dependency on temperature of the saturation vapor pressure e_s, of the latent heat L, and of the heat capacities C_{pv} and C_l. Our purpose here is to further simplify the equation of state so that the sole nonlinearity remaining in the equation of state is that associated with phase transitions. In order to do so, we follow [5, 6] by assuming that the entropy and moisture in the system are close to the reference value S_{ref} and $q_{T,ref}$ and that the partial derivatives of the buoyancy with respect to the entropy and to total water content depend only on whether a parcel is saturated or not:

$$\left(\frac{\partial B}{\partial S}\right)_{q_T,z} = \frac{g}{\alpha_{ref}}\left(\frac{\partial \alpha}{\partial S}\right)_{q_T,p} = \begin{cases} B_{S,u} & \text{if } q_T \leq q_{sat}(S,z) \\ B_{S,s} & \text{if } q_T > q_{sat}(S,z) \end{cases} \tag{3.6}$$

$$\left(\frac{\partial B}{\partial q_T}\right)_{S,z} = \frac{g}{\alpha_{ref}}\left(\frac{\partial \alpha}{\partial q_T}\right)_{S,p} = \begin{cases} B_{q_T,u} & \text{if } q_T \leq q_{sat}(S,z) \\ B_{q_T,s} & \text{if } q_T > q_{sat}(S,z). \end{cases} \tag{3.7}$$

The four quantities $B_{S,u}$, $B_{S,s}$, $B_{q_T,u}$ and $B_{q_T,s}$ are taken to be constant throughout the domain.

Once we have fixed the partial derivatives of the buoyancy in the saturated and unsaturated regions, the conserved variables q_T and S can be combined into two new variables D and M

$$D = B_{S,u}(S - S_{ref}) + B_{q_T,u}(q_T - q_{T,ref}) \tag{3.8}$$
$$M = B_{S,s}(S - S_{ref}) + B_{q_T,s}(q_T - q_{T,ref}). \tag{3.9}$$

Note that, by definition, the reference profile corresponds to $M_{ref}(z) = 0$ and $D_{ref}(z) = 0$. These two variables are such that the variations of the buoyancy are controlled solely by the 'saturated' or 'moist buoyancy' M in the saturated regions, and by the 'unsaturated' or 'dry buoyancy' D in the unsaturated regions. Indeed, for an unsaturated parcel, we have then

$$\left(\frac{\partial B}{\partial D}\right)_{M,z} = 1, \text{ and } \left(\frac{\partial B}{\partial M}\right)_{D,z} = 0, \tag{3.10}$$

while for a saturated parcel, we have

$$\left(\frac{\partial B}{\partial D}\right)_{M,z} = 0, \text{ and } \left(\frac{\partial B}{\partial M}\right)_{D,z} = 1. \tag{3.11}$$

These two variables D and M can be thought of as the equivalent of the liquid water potential temperature θ_l and the equivalent potential temperature θ_e that are used in meteorology.

3.3. Saturation condition. The buoyancy of any parcel can obtained by integrating the partial derivatives (3.10)–(3.11) and by taking advantage of the fact that the buoyancy of the reference state is zero, i.e., $B(M_{ref} = 0, D_{ref} = 0) = 0$. However to do so we must first establish a criterion which determines whether the parcel is saturated or not. We need a condition of the form

$$F(M, D, z) \geq 0, \tag{3.12}$$

for which a parcel is saturated. When $F(M, D, z) = 0$, the parcels are said to be on the saturation line, in the sense that such a parcel can be made either saturated or unsaturated by an infinitesimal change of its current thermodynamic state. The condition (3.12) can be obtained directly by linearizing the equation of state for moist air. A more intuitive approach will be discussed here. First, let us consider two parcels (M_1, D_1) and (M_2, D_2) on the saturation line at a given height z, as illustrated in figure 3.1. The buoyancy difference between the two parcels can be obtained by either following a saturated path – first increasing the moist buoyancy M and then increasing the dry buoyancy D – or by following an unsaturated path – first increasing the dry buoyancy D and then increasing the moist buoyancy M. Given the partial derivatives (3.10) and (3.11) in the saturated and unsaturated regions, the first path implies that the buoyancy difference between the two parcels is $B_2 - B_1 = M_2 - M_1$, while the second path yields $B_2 - B_1 = D_2 - D_1$. This means that $M_2 - M_1 = D_2 - D_1$ or that the slope of the saturation line has to be one. For the buoyancy to be continuous, the saturation line must be defined by

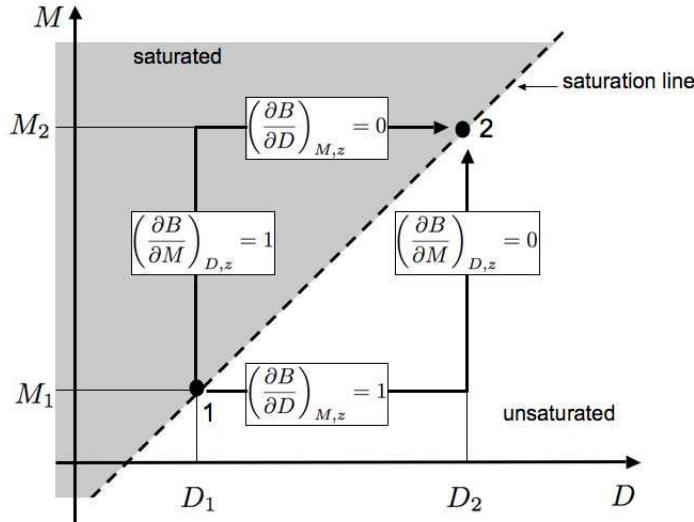$$F(M, D, z) = M - D - f(z) = 0. \tag{3.13}$$

FIG. 3.1. *Schematic representation for the derivation of the slope of the saturation line* (3.13). *Parcels 1 and 2 are on the saturation line. The buoyancy difference between the two parcels, $B_2 - B_1$, can be obtained by following a trajectory that lies in the saturated portion of the domain (above the saturation line), or one that lies in the unsaturated portion (below the saturation line). The unity slope of the saturation line* (3.13) *results from requiring that the buoyancy difference is independent of the path followed.*

The expression contains a yet unknown function $f(z)$ which we determine in the following. We construct a cycle in the vicinity of the saturation line as sketched in figure 3.2. The four steps of the cycle are partly in an unsaturated and saturated environment obeying Γ_u and Γ_s, the unsaturated and saturated adiabatic lapse rates. They are defined as

$$\Gamma_u = -\left(\frac{\partial T}{\partial z}\right)_{S,q_T,q_T < q_s} \tag{3.14}$$

$$\Gamma_s = -\left(\frac{\partial T}{\partial z}\right)_{S,q_T,q_T > q_s}. \tag{3.15}$$

As stated above, the reference level z_{ref} is defined as $M = D = 0$ and thus $f(z_{ref}) = 0$. The temperature is $T = T_{ref}$. The cycle consists of the following four steps.

- Step I: A saturated parcel rises adiabatically from $z = z_{ref}$ (point 1) to $z = z_1$ (point 2) in a saturated environment. The adiabatic phase change leaves the buoyancy B unchanged and $D = M = B = 0$ at point 2. The temperature changes to $T = T_{ref} - \Gamma_s(z_1 - z_{ref})$.

- Step II: D increases to D_{sat} by removing liquid water from the moist air parcel while maintaining a constant buoyancy. As changing D in a saturated region does not change the buoyancy, the parcel has still $B = M = 0$ at point 3. T remains (nearly) unchanged in comparison to point 2.
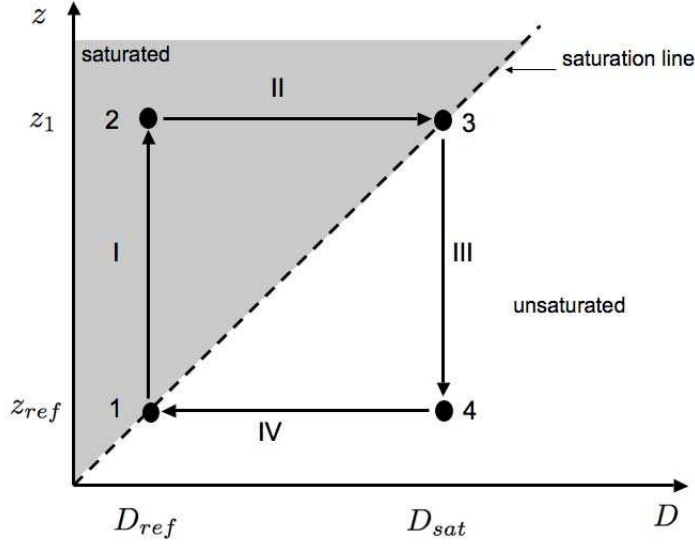
FIG. 3.2. *Illustration of a cycle for a moist air parcel in a partly saturated and unsaturated environment.*

- Step III: Adiabatic descent from $z = z_1$ back to $z = z_{ref}$ is carried out in the unsaturated region. At point 4, $M = 0$, $B = D = D_{sat}$. The temperature increases to $T = T_{ref} - \Gamma_s(z_1 - z_{ref}) + \Gamma_u(z_1 - z_{ref})$. The buoyancy gain results to

$$B \approx g \frac{T - T_{ref}}{T_{ref}} = g \left(\frac{\Gamma_u - \Gamma_s}{T_{ref}} \right) (z_1 - z_{ref}), \tag{3.16}$$

- Step IV: The air parcel is moistened in an unsaturated environment and returns from point 4 to the starting point 1. The temperature remains nearly at the value at point 4 and $M = 0$ (since the moist buoyancy remains unchanged if the path is in the unsaturated region). Thus we end with $B = -D_{sat}$ at the starting point 1 and the saturation line.

As a consequence of (3.13), we have that $D_{sat} = f(z)$. This is also the buoyancy gained by an saturated adiabatic displacement from z_1 to z_{ref}, i.e., with (3.16) we obtain

$$D_{sat} = f(z) = N_s^2 (z - z_{ref}), \tag{3.17}$$

where the quantity N_s corresponds to the Brunt-Vaisala frequency of a moist adiabatic temperature profile. It is given by

$$N_s^2 = \frac{g}{T_{ref}} (\Gamma_u - \Gamma_s). \tag{3.18}$$

For Earth-like conditions, N_s^2 is on the order of $10^{-4} s^{-2}$.

A similar cycle can be constructed in order to find the expression for M_{sat}. A parcel becomes then unsaturated as it moves down from the saturation line to $z_2 <$

z_{ref}. When this parcel is brought back to the level z_{ref}, its buoyancy is given $B = M_{sat} = N_s^2(z_{ref} - z_2)$. The definition of M_{sat} and D_{sat} can be extended above and below the level z_{ref}

$$D_{sat}(z) = \begin{cases} 0 & \text{for } z \leq z_{ref} \\ N_s^2(z - z_{ref}) & \text{for } z > z_{ref} \end{cases} \tag{3.19}$$

$$M_{sat}(z) = \begin{cases} N_s^2(z_{ref} - z) & \text{for } z \leq z_{ref} \\ 0 & \text{for } z > z_{ref}. \end{cases} \tag{3.20}$$

Note that the parcel with $(M = M_{sat}(z), D = D_{sat}(z))$ is on the saturation line and has a buoyancy $B = 0$ at level z. Using the values for M_{sat} and D_{sat} in the saturation criterion (3.12) yields the condition for saturation

$$M - D \geq N_s^2(z_{ref} - z). \tag{3.21}$$

The buoyancy of a parcel is then given by

$$B(M, D, z) = \begin{cases} D - D_{sat}(z) & \text{if } M - D < N_s^2(z_{ref} - z) \\ M - M_{sat}(z) & \text{otherwise.} \end{cases} \tag{3.22}$$

Without loss of generality, we can impose the reference state to be saturated at level $z_{ref} = 0$. In this case, the expression (3.22) for the buoyancy can be written as

$$B(M, D, z) = \max(M, D - N_s^2 z). \tag{3.23}$$

Figure 3.3 illustrates the dependence of the buoyancy on D and M at a given level. The saturation line (indicated as dashed line) always has a slope of one and separates the saturated and unsaturated regions. Lines of constant buoyancy are parallel to the M-axis in the unsaturated region and parallel to the D-axis in the saturated regions. The complete system of equations can now be written as follows:

$$\frac{d\mathbf{u}}{dt} = -\nabla p' + B\mathbf{k} + \nu\nabla^2\mathbf{u} \tag{3.24a}$$

$$\nabla \cdot \mathbf{u} = 0 \tag{3.24b}$$

$$\frac{dD}{dt} = \dot{D} + \kappa\nabla^2 D \tag{3.24c}$$

$$\frac{dM}{dt} = \dot{M} + \kappa\nabla^2 M, \tag{3.24d}$$

with the buoyancy given by (3.23). By preserving the discontinuity in its partial derivative, the simplified state equation provides a thermodynamically consistent description of phase transition. The Boussinesq system (3.23)–(3.24d) provides a very simple analogue for atmospheric moist convection while still accounting for the effect of phase transition. The model does not allow for the condensed water to fall out.

The unsaturated and saturated buoyancies D and M are two state variables that are conserved for reversible adiabatic processes and are such that the density can be obtained as a function of D and the pressure p for an unsaturated parcel, and as a function of M and the pressure p for a saturated one. As such, D and M are nontrivial functions of the entropy and total water content of the moist air. Rather than providing an exact physical equivalent for D and M we will provide a physical interpretation to offer some intuition while avoiding the more technical aspects of moist thermodynamics.
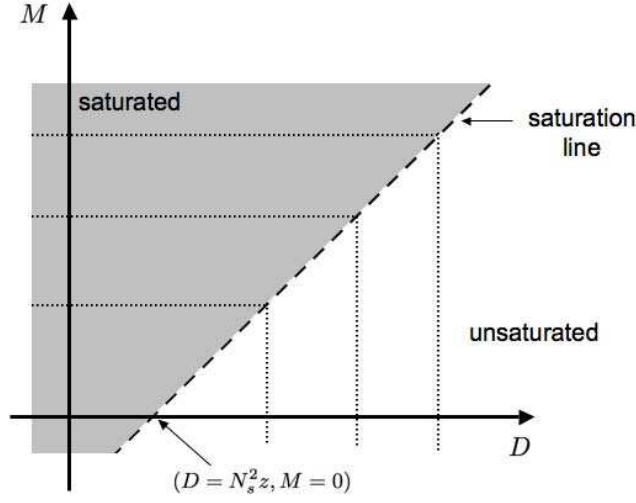
FIG. 3.3. *Buoyancy as a function of the two variables D and M at a given height z. Dotted lines are lines of constant buoyancy. The saturation line (dashed line) indicates the separation between the saturated and unsaturated parcels. The saturation line intersects the D-axis at $(D = N_s^2 z, M = 0)$ corresponding to a parcel on a saturated line with the same buoyancy as the reference state $(D = 0, M = 0)$.*

First, if we neglect on first order the changes of density due to the changes in the concentration of water vapor or liquid water content, the buoyancy is proportional to the temperature fluctuation

$$B = g \left[\frac{T - T_{ref}(z)}{T_{ref}(z)} + \epsilon(q_v - q_{v,ref}) - q_l \right] \approx g \frac{T - T_{ref}(z)}{T_{ref}(z)}, \qquad (3.25)$$

with $\epsilon = 0.608$. For a compressible fluid however, temperature is not an adiabatic invariant. Rather, two quantities, known as the *dry static energy* $s = C_p T + gz - L_v q_l$ and the *moist static energy* $h = C_p T + gz + L_v q_v$ [8] can be shown to be approximately conserved for reversible adiabatic motions. Furthermore, for an unsaturated parcel, there is no liquid water $q_l = 0$ and the variations of temperature are directly related to the variation of dry static energy. This implies that the unsaturated buoyancy D is related to the changes in dry static energy:

$$D \sim C_p T + gz - L_v q_l. \qquad (3.26)$$

Similarly, for a saturated parcel at a given pressure, the amount of water vapor present should be a function of temperature alone through the Clausius-Clapeyron relationship. This means that temperature can be obtained for the moist static energy, and thus that the saturated buoyancy M is related to the moist static energy

$$M \sim C_p T + gz + L_v q_v. \qquad (3.27)$$

The difference of M and D is proportional to the total water content of the parcel

$$M - D \sim q_T - q_{T,ref}. \qquad (3.28)$$

For an *unsaturated* parcel with $M - D \leq -N_s^2 z$, only water vapor is present, and we have thus

$$q_v - q_{T,ref} \sim M - D \quad \text{and} \quad q_l = 0. \tag{3.29}$$

When a parcel is *saturated*, the amount of condensed water is proportional to how much $M - D$ exceeds the saturation condition, i.e.:

$$q_l \sim M - D + N_s^2 z. \tag{3.30}$$

The Boussinesq approximation at the basis of the system (3.23)–(3.24d) is based on an expansion of the governing equation in terms of the density fluctuations. It is only accurate under the following conditions: (1) the density fluctuations must be small, i.e., $B \ll g$; (2) the Mach number U_f / c_s, defined as the ratio of a typical velocity scale U_f to the speed of sound c_s, is small $U_f / c_s \ll 1$; (3) the vertical extent of the domain must be small in comparison to the density scale height. The latter in the atmosphere is approximately 8 km, which means that the Boussinesq approximation is not accurate for simulating atmospheric flow deeper than 2-3 km. Flows on deeper layers can be handled by the anelastic approximation [23, 16, 7, 1]. The use of the piecewise linear equation of state introduces an additional limitation. The derivation of (3.23) assumes that the partial derivatives of the buoyancy depend only on whether a parcel is saturated or not (equations (3.6)–(3.7)). This neglects, among other things, variations in the saturated lapse rate Γ_s and in the saturated Brunt-Vaisala frequency N_s with water content and temperature. The saturation specific humidity q_s is highly sensitive to temperature, and thus exhibits strong vertical variation. The scale height for q_s is approximately 3 kilometers in the Earth atmosphere. This implies that the piecewise linear equation of state can only be accurate for shallow flow, for layer shallower than 1km. For thicker layers, the piecewise linear equation of state (3.23) still offers a self-consistent description of a 'moist' fluid with phase transition, but it should not be viewed as a quantitative representation of moist air.

4. Numerical studies in idealized moist Rayleigh-Bénard convection

4.1. Stationary solution and dimensionless parameters. An idealized moist Rayleigh-Bénard problem is presented now which is based on the piecewise linear Boussinesq system (3.23)–(3.24d) with $\dot{D} = \dot{M} = 0$. The is similar to the classic Rayleigh-Bénard system except for the fact that the equation of state used here allows for phase transitions. Figure 4.1 illustrates the basic configuration. We consider a laterally extended layer of fluid bounded by two planes at the bottom $z = 0$ and top $z = H$. This situation might be similar to the conditions that prevail in regions of stratiform convection often observed over subtropical oceans: the lower boundary corresponds to the ocean surface, and the upper-boundary can be interpreted as a simplified representation of the sharp potential temperature increase at the top of cloudy layer. The fluid is destabilized by imposing fixed values of D and M at the upper and lower boundaries

$$D(0) = D_0 \tag{4.1a}$$
$$D(H) = D_H \tag{4.1b}$$
$$M(0) = M_0 \tag{4.1c}$$
$$M(H) = M_H. \tag{4.1d}$$

The free-slip (or stress-free) boundary condition holds for the velocity field at both planes and reads

$$\frac{\partial u_x}{\partial z} = \frac{\partial u_y}{\partial z} = 0 \quad \text{and} \quad u_z = 0. \tag{4.2}$$

Similar boundary conditions have been used in [14, 15, 5, 6]. Alternative boundary conditions can be implemented, for example by prescribing constant flux for both D and M, which in practice are determined by the normal derivatives $\partial D/\partial z$ and $\partial M/\partial z$. The influence of the change in boundary conditions on the turbulent heat (or buoyancy) transport is still a matter of current research. A three-dimensional numerical study of dry convection in a cylindrical cell with a constant flux boundary condition at the bottom and a constant buoyancy at the top detected a smaller heat transport in comparison to two fixed buoyancy boundary conditions for Rayleigh numbers $Ra > 10^9$ [34]. However, in a two-dimensional numerical simulation of dry convection with two fixed flux boundary conditions no differences in the turbulent heat transport appeared for $Ra \geq 10^7$ [12]. It thus remains to determine how the geometry or the spatial dimension affects the heat transport.

The problem has a stationary solution where there is no motion ($\mathbf{u} = 0$), and the state variables D and M are linear functions of height

$$\overline{D}(z) = D_0 + \frac{D_H - D_0}{H} z \tag{4.3a}$$

$$\overline{M}(z) = M_0 + \frac{M_H - M_0}{H} z. \tag{4.3b}$$

This solution may be partially saturated and partially unsaturated. Equation (3.23) indicates that the interface between the saturated and unsaturated regions follows from the condition $\overline{M}(z) = \overline{D}(z) - N_s^2 z$. This interface — the cloud base — is located at the level $z = z_{CB}$ and given by

$$z_{CB} = \frac{(M_0 - D_0)H}{D_H - D_0 - M_H + M_0 - N_s^2 H}. \tag{4.4}$$

The air is saturated wherever $\overline{M}(z) > \overline{D}(z) - N_s^2 z$, and unsaturated otherwise. In figure 4.1 this is the case for height $z_{CB} \leq z \leq H$. Cloudy air will fill the upper part of the layer if $M_H - M_0 - D_H + D_0 + N_s^2 H > 0$. It is also possible that the steady solution is exactly at the saturation point in the entire domain, i.e., $\overline{M}(z) - \overline{D}(z) = -N_s^2 z$ for all $z \in [0, H]$. Any small perturbation yields a saturated or unsaturated parcel then. This particular situation is exactly the one which has been investigated by Bretherton [5, 6]. To our knowledge it is the sole investigation of the moist Rayleigh-Bénard problem under the framework proposed here.

The problem can be made dimensionless. The dry and moist buoyancy fields are therefore decomposed as

$$D(\mathbf{x}, t) = \overline{D}(z) + D'(\mathbf{x}, t) \tag{4.5}$$

$$M(\mathbf{x}, t) = \overline{M}(z) + M'(\mathbf{x}, t). \tag{4.6}$$

The variations about the mean profiles of both fields have to vanish at $z = 0$ and H, which imposes the boundary conditions $D' = 0$ and $M' = 0$. A nondimensional version of the equations is obtained by defining the nondimensional variables (noted by an
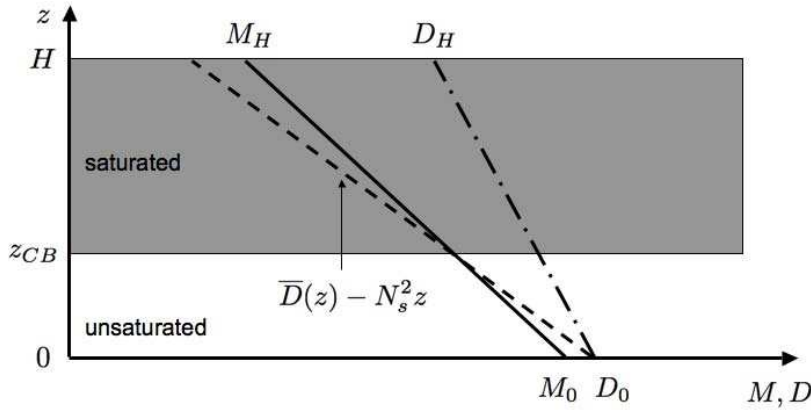
FIG. 4.1. *Steady solution for the idealized moist Rayleigh-Bénard problem in an infinitely extended layer of height H. The vertical profiles for the two state variables $\overline{D}(z)$ (dash-dotted line), $\overline{D}(z) - N_s^2 z$ (dashed line) and $\overline{M}(z)$ (solid line) are shown. The interface between the unsaturated and saturated regions is located at the level $z = z_{CB}$.*

asterisk)

$$\mathbf{u}^* = [U_f]^{-1}\mathbf{u}$$
$$(x^*, y^*, z^*) = H^{-1}(x, y, z)$$
$$t^* = \frac{[U_f]}{H}t$$
$$p^* = [U_f]^{-2}p'$$
$$(B^*, D^*, M^*) = [B]^{-1}(B, D, M)$$

Here, $[B]$ is the characteristic buoyancy and $[U_f]$ the free-fall velocity. They are given by

$$[B] = M_0 - M_H$$
$$[U_f] = \sqrt{H|M_0 - M_H|}.$$

The dimensionless version of equations (3.24a)–(3.24d) together with the decompositions (4.5) and (4.6) is

$$\frac{d\mathbf{u}^*}{dt^*} = -\nabla_* p^* + B^*(M^*, D^*, z^*)\mathbf{k} + \sqrt{\frac{Pr}{Ra_M}}\nabla_*^2 \mathbf{u}^* \tag{4.7a}$$

$$\nabla_* \cdot \mathbf{u}^* = 0 \tag{4.7b}$$

$$\frac{dD'^*}{dt^*} = \frac{1}{\sqrt{PrRa_M}}\nabla_*^2 D'^* + \frac{Ra_D}{Ra_M}u_z^* \tag{4.7c}$$

$$\frac{dM'^*}{dt^*} = \frac{1}{\sqrt{PrRa_M}}\nabla_*^2 M'^* + u_z^*. \tag{4.7d}$$

Here, $\frac{d}{dt^*} = \frac{\partial}{\partial t^*} + \mathbf{u}^* \cdot \nabla_*$ denotes the nondimensional version of the material derivative, while ∇_* and ∇_*^2 are the dimensionless gradient and Laplacian operators. These

equations contain three nondimensional parameters. As the diffusivities of both buoyancy fields are the same there is only one Prandtl number, which is defined as

$$Pr = \frac{\nu}{\kappa}. \tag{4.8}$$

In our studies, this will take the value of air, i.e., $Pr = 0.7$. This problem is also characterized by two Rayleigh numbers, Ra_D and Ra_M, which quantify the driving of the unsaturated and saturated fields D and M

$$Ra_D = \frac{H^3(D_0 - D_H)}{\nu\kappa} \tag{4.9}$$

$$Ra_M = \frac{H^3(M_0 - M_H)}{\nu\kappa}. \tag{4.10}$$

Typical values of the Rayleigh numbers for atmospheric flows range from 10^{18} to 10^{22}. Under most circumstances, the amount of water in the atmosphere decreases with height. This implies that the moist Rayleigh number should be larger than the dry Rayleigh number: $Ra_M \geq Ra_D$. Furthermore, it is often observed that the atmosphere is stable for unsaturated parcels, but unstable for saturated parcels. This is known in meteorology as conditional instability, and corresponds to having a positive value of the moist Rayleigh number ($Ra_M > 0$) number, but a negative value of the dry Rayleigh number ($Ra_D < 0$).[2] Conditional instability is an important aspect of atmospheric dynamics that is specifically tied to the phase transition.

In addition to the three parameters explicitly present in equations (4.7a)–(4.7d), two more parameters are implicitly hidden within the definition of the buoyancy B^*. The dimensional buoyancy (3.23) can be re-written as

$$B = \overline{M}(z) + \max\left(M', D' + \overline{D}(z) - \overline{M}(z) - N_s^2 z\right)$$
$$= M_0 + \frac{M_H - M_0}{H}z + \max\left(M', D' + (D_0 - M_0) + \frac{D_H - D_0}{H}z - \frac{M_H - M_0}{H}z - N_s^2 z\right).$$

Note that the first two terms on the right-hand side are horizontally uniform. This implies that they can be balanced by a horizontally uniform pressure field given by $p(z) = -M_0 z - \frac{M_H - M_0}{2H}z^2$. We can thus remove the first two terms from the buoyancy field without any loss of generality. In this case, the dimensionless buoyancy becomes

$$B^* = \max\left(M'^*, D'^* + SSD + \left(1 - \frac{Ra_D}{Ra_M}\right)z^* - CSAz^*\right). \tag{4.11}$$

The two nondimensional parameters here are the *Surface Saturation Deficit* (*SSD*) and the *Condensation in Saturated Ascent* (*CSA*) defined as

$$SSD = \frac{D_0 - M_0}{M_0 - M_H} \tag{4.12}$$

$$CSA = \frac{N_s^2 H}{M_0 - M_H}. \tag{4.13}$$

These two new nondimensional parameters respectively measure how close the lower boundary is to being saturated and how much water can condense within the atmospheric layer. When $D_0 - M_0$ is positive, the air at the lower boundary is unsaturated

---

[2]The reverse case, with $Ra_D > 0$ and $Ra_M < 0$, is possible but rather exceptional, corresponding to situations where mammatus clouds form in the outflow of deep convective towers.

and $D_0 - M_0$ is proportional the "water deficit", i.e., the amount of water vapor that must be added for the parcel to become saturated. Conversely, if $D_0 - M_0$ is negative, the air at the lower boundary is saturated and $M_0 - D_0$ is proportional to the amount of condensed water present. A positive value of SSD indicates that the lower boundary is unsaturated and would occur over the continents. For convection over the ocean, one can assume that the lower boundary is saturated with $SSD = 0$.

The dimensionless CSA is related to the drop in concentration of water vapor at saturation between the bottom ($z = 0$) and the top ($z = H$) of the layer. The quantity $N_s^2 H$, used to define CSA, is proportional to the amount of condensation that takes place when a parcel is lifted from the bottom. It is also the amount of buoyancy that can be gained by a saturated parcel. Consider two parcels starting at the bottom with the same buoyancy. The first parcel is lifted along a saturated trajectory, while the second parcel is lifting without any condensation taking place (for example, the first parcel has $D = M = 0$, while the second has $D = 0, M = -N_s^2 H$). At the top of the domain, the buoyancy of the first parcel will be larger than of the second parcel by $N_s^2 H$. The CSA can be interpreted as the total amount of latent heat released by condensation when a saturated parcel ascent from the bottom to the top of the domain normalized by the difference in moist static energy between the bottom and the top of the domain. A large value of the CSA implies that the amount of cloud water that can be formed is large when compared to horizontal fluctuation variations of the water vapor content. This indicates the presence of an unbroken cloud layer, similar to the stratocumulus cloud regime found in the Eastern portions of the tropical oceans. Conversely, a small value of CSA indicates that horizontal fluctuations of water vapor content are large compared to the cloud water content, i.e., that isolated clouds can be present.

For a somewhat more intuitive interpretation of these two nondimensional parameters, one can think in term of the location and shape of the cloud base. A parcel with given value of M and D is unsaturated below a level $z = (D - M)/N_s^2$, and saturated above. In the moist Rayleigh-Bénard problem, different parcels have different saturation levels, so that the cloud base varies. One can however use the saturation level associated with parcels originating from the lower and upper boundary to infer the location and variability of the cloud base in the convective layer. We define $z_{CB}^{(0)}$ as the levels at which a parcel originating from the lower boundary (with $M = M_0$ and $D = D_0$) first becomes saturated. Notice here that this level is given by

$$\frac{z_{CB}^{(0)}}{H} = \frac{D_0 - M_0}{N_s^2 H} = \frac{SSD}{CSA}$$

and depends only on CSA and SSD. Similarly, if $z_{CB}^{(H)}$ is the level at which a parcel from the upper boundary (with $M = M_0$ and $D = D_0$) becomes unsaturated, then we have

$$\frac{z_{CB}^{(H)}}{H} = \frac{D_H - M_H}{N_s^2 H} = \frac{SSD + 1 - \frac{Ra_D}{Ra_M}}{CSA}.$$

For given values of the two Rayleigh numbers Ra_D and Ra_M, the location and fluctuations of the cloud base are thus determined by the SSD and CSA.
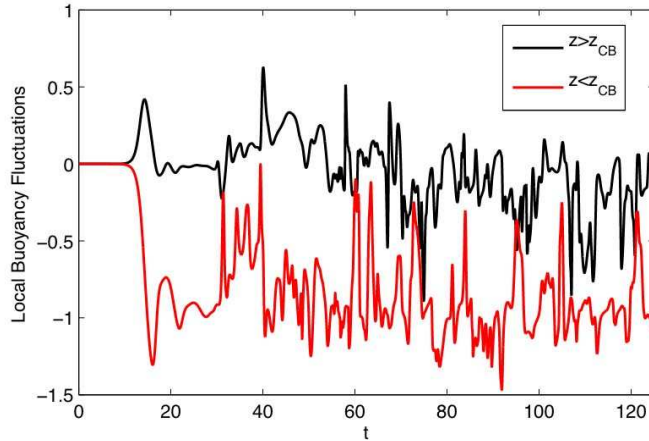
FIG. 4.2. *Time traces of the buoyancy fluctuations B' at two particular grid points, one above and one below the cloud base. Data are taken from run MRB1.*
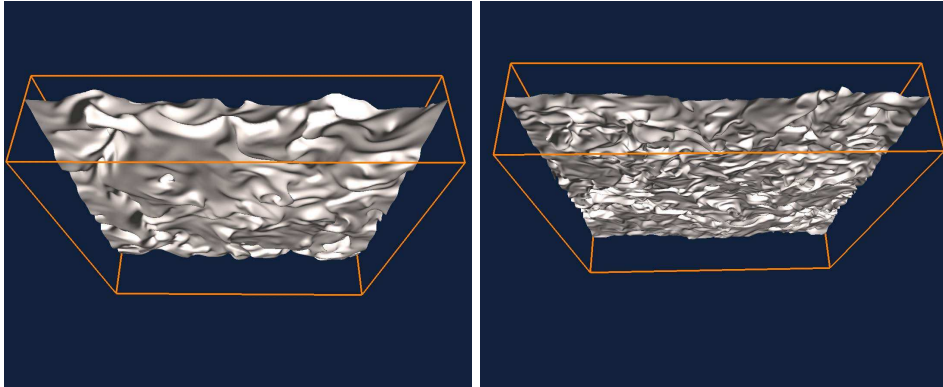

FIG. 4.3. *Clouds, defined as $M - D + N_s^2 z \geq 0$. Data is taken from a snapshot of runs MRB3 (left) and MRB4 (right). The view perspective is from below into the slab $V = L^2 H$. The cloud base is unbroken and cloudy air is found above the shown isosurface.*

4.2. Numerical model and results.   For sufficiently large Rayleigh numbers an initial small perturbation of the static solution leads to turbulent motion in the layer. This nonlinear evolution is studied in the following by direct numerical simulations (DNS) of equations (3.23)–(3.24d). In DNS, neither turbulent eddy viscosities nor subgrid-scale parametrizations are applied, which limits the range of accessible Rayleigh numbers.

The dry and moist buoyancy fields are decomposed in terms of their perturbations D' and M' and linear profiles $\overline{D}$ and $\overline{M}$, as defined in (4.5)–(4.6). The same decomposition follows for the total buoyancy B. The mean buoyancy variations depend on the vertical coordinate z only. They can be balanced by an additional pressure contribution (see (4.11)). The combination of (3.23) and $\overline{B} = \max(\overline{M}, \overline{D} - N_s^2 z)$ results in four different cases for the local buoyancy fluctuation $B'(\mathbf{x}, t)$ which enters
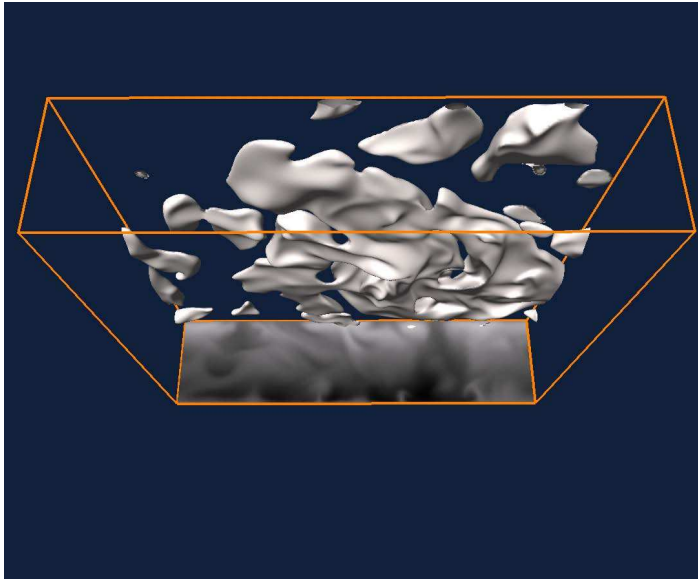
FIG. 4.4. *Isosurface of the buoyancy fluctuation $B' = 1.2$. Data is taken from a snapshot of run MRB3. The view perspective is again from below into the slab. In addition a greyscale contour plot of B' is at the backside of the slab.*

the momentum balance. Note, that the field B' has to be evaluated from D and M at each time step and for each grid point. Figure 4.2 shows two such time series of the buoyancy fluctuations, one at a point above the (prescribed) cloud base z_{CB} and one below.

All turbulent fields are expanded in finite Fourier series with respect to x and y directions and in sines or cosines with respect to z. Lateral boundary conditions are periodic. The finite lateral extension introduces a further geometric parameter to the problem. The simulation volume, $V = L^2 H$, has an aspect ratio which is defined as

$$A = \frac{L}{H}, \tag{4.14}$$

where L is the length with respect to x and y directions. In the context of atmospheric science $A \gg 1$ is a desirable configuration. In the following numerical experiments, it will be held fixed at $A = 4$. The Fourier expansion of all fields allows the use of the pseudospectral method [24, 29] with a 2/3 de-aliasing rule for the Fast Fourier Transforms. The advancement in time is done by a second-order Runge-Kutta scheme. In Table 1, we summarize the parameters of the different runs. We list two dry reference runs DRB1 and DRB1a. The moist convection runs MRB1, MRB2 and MRB3 differ in the cloud base z_{CB} and the Surface Saturation Deficit SSD. Runs MRB3 and MRB4 have the same set of parameters, except for both Rayleigh numbers Ra_D and Ra_M. The increase of Ra_D and Ra_M by a factor of 10 requires a doubling of the number of grid points in each space direction.

Clouds in the simulations occur whenever a parcel is saturated for $M - D + N_s^2 z \geq 0$. Figure 4.3 shows the bases of the cloud layer in simulations MRB3 (left) and MRB4 (right). The larger the Rayleigh numbers, the smaller the height variations of the cloud base. Saturated parcels are located in the upper portion of the domain.

Run	Ra_D	Ra_M	Pr	SSD	z_{CB}/H	CSA	U_f	A	$\langle u_i^2 \rangle_{V,t}$
DRB1	7.0×10^5	–	0.7	–	–	–	2.63	4	1.00
DRB1a	9.5×10^5	–	0.7	–	–	–	3.06	4	1.22
MRB1	7.0×10^5	9.5×10^5	0.7	0.05	0.2	0.53	3.06	4	1.16
MRB2	7.0×10^5	9.5×10^5	0.7	0.10	0.4	0.53	3.06	4	1.13
MRB3	7.0×10^5	9.5×10^5	0.7	0.18	0.7	0.53	3.06	4	1.03
MRB4	7.0×10^6	9.5×10^6	0.7	0.18	0.7	0.53	3.06	4	0.83

TABLE 4.1. *Parameters of the direct numerical simulations. The computational grid contains $N_x \times N_y \times N_z = 256 \times 256 \times 65$ grid points for all cases except MRB4. Run MRB4 is conducted on a $N_x \times N_y \times N_z = 512 \times 512 \times 129$ grid. In this series of simulations we have varied the surface saturation deficit SSD of the convective layer only. The CSA is constant. Run DRB1a is conducted for a comparison of the buoyancy statistics. The free-fall velocity for the dry convection runs is given by $U_f = \sqrt{H|D_0 - D_H|}$. Note that $\langle u_i^2 \rangle_{V,t}$ is a volume and time average of the velocity magnitude square.*

In all moist simulations, the upper portion of the domain is entirely saturated. In other words, our simulations are similar to the stratocumulus regime, where the cloud layer is not broken into individual cumulus clouds. All simulations are within the so-called soft-turbulence regime of thermal convection which holds for Rayleigh numbers $Ra_D \lesssim 10^7 - 10^8$. Note that Rayleigh numbers in the atmospheric boundary layer exceed the ones of our model by about 10 order of magnitude. Nevertheless, figure 4.4 illustrates a complex three-dimensional structure for the buoyancy fluctuations.

Figure 4.5 (left) compares the turbulent kinetic energy $E_{kin}(t) = 1/(2V) \int_V u_i^2 dV$ for the dry Rayleigh-Bénard convection reference run (DRB1) with the moist cases MRB1 – MRB3, which differ in the SSD with respect to each other. After the initial growth of the infinitesimal perturbations about the linear buoyancy profiles, the system passes through a phase of strong relaxation oscillations before reaching a statistically stationary state of turbulent convection for $t \geq 75$. It is found that the time average of the turbulent kinetic energy is increasing with decreasing SSD (see figure 4.5 and the values in the table). It can therefore be concluded that the phase changes have an impact on the velocity fluctuations, since a smaller SSD increases the fraction of cloudy air. The inset of the panel of figure 4.5 shows that the growth rate toward a turbulent state increases for increasing Ra.

The two buoyancy fields are advected by the same turbulent flow and follow linear equations. Therefore, they can be combined to a new scalar field

$$\phi(\mathbf{x},t) = H \left(\frac{M'(\mathbf{x},t)}{M_H - M_0} - \frac{D'(\mathbf{x},t)}{D_H - D_0} \right). \tag{4.15}$$

The field has a dimension of length, $\phi^*(\mathbf{x}^*,t^*) = \phi(\mathbf{x},t)/H$. In dimensionless form the scalar is given by

$$\phi^*(\mathbf{x}^*,t^*) = \left(\frac{Ra_M}{Ra_D} D'^*(\mathbf{x}^*,t^*) - M'^*(\mathbf{x}^*,t^*) \right). \tag{4.16}$$

Equations (3.24c) and (3.24d) consequently yield an advection-diffusion equation for a decaying passive scalar ϕ

$$\frac{\partial \phi}{\partial t} + (\mathbf{u} \cdot \nabla)\phi = \kappa \nabla^2 \phi. \tag{4.17}$$
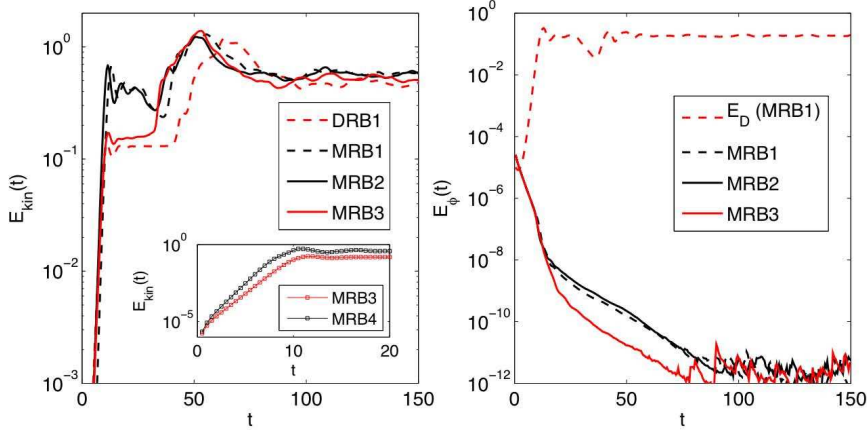
FIG. 4.5. *Left: Turbulent kinetic energy $E_{kin}(t)$ for the three moist convection runs and the dry reference run DRB1. The mean square turbulent velocities were determined for $t > 75$ and are listed in table 1. The inset compares the initial growth phase of the turbulence for runs MRB3 and MRB4 starting with exactly the same form of the small perturbation of the static equilibrium. Right: Scalar variance $E_\phi(t)$ for the three moist convection runs (see equation (4.18)). For comparison we add the graph of the variance of the dry buoyancy field $E_D(t)$ which is defined the same way as $E_\phi(t)$ (see equation (4.18)).*

In other words, the dynamics of both buoyancy fields gets synchronized with advancement in time. The right plot of figure 4.5 indeed shows that the corresponding scalar variance for the moist runs, which is given by

$$E_\phi = \frac{1}{2V} \int_V \phi^2 \mathrm{d}V, \qquad (4.18)$$

decays to zero while the scalar variances of M and D remain statistically stationary. The decay is found to be exponential with two different slopes. A very steep decay is connected with the initial growth of the small perturbation for D and M. A less steep decay takes over when the growth of both buoyancy fields saturates and relaxes into the statistically stationary turbulent state. This continues until the (single precision) noise level is reached. The dynamics of ϕ is altered when additional volume forcing terms are added to the model. Those can mimic radiative cooling effects. Further complexity arises if we allow different scalar diffusivities of D and M. Then the dynamics of so-called differential diffusion comes into play [28]. Both aspects are interesting extensions of the present model and will be studied elsewhere.

Figure 4.6(a) reports our findings for the turbulent transport properties across the convection layer. The buoyancy flux $\langle u_z B'(z) \rangle$ is plotted for the different runs. The profiles are obtained from 31 statistically independent samples where the fields are averaged in lateral planes. The corresponding time interval is again $t \geq 75$ (see figure 4.5). The presence of cloudy air and latent heat release causes a flux increase in the upper region of the layer. In the moist simulation, the buoyancy flux profile shows a sharp increase near the middle of the domain. Indeed, when all the parcels in a layer are unsaturated, the buoyancy flux is given by the flux of the 'dry buoyancy': $\langle u_z B'(z) \rangle = \langle u_z D'(z) \rangle$. In contrast, in a layer where all the parcels are saturated, it is equal to the flux of 'moist buoyancy': $\langle u_z B'(z) \rangle = \langle u_z M' \rangle(z)$. In our simulations, the
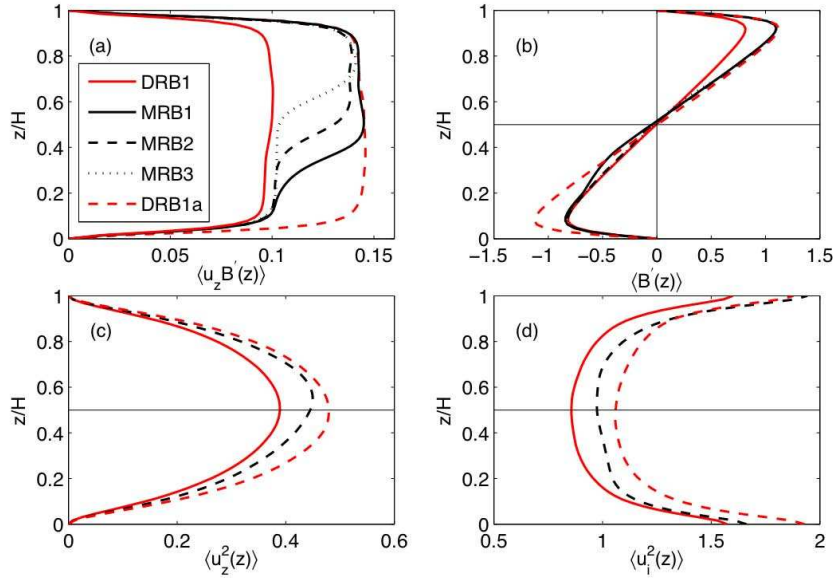
FIG. 4.6. *(a) Vertical profiles of the mean buoyancy flux $\langle u_z B' \rangle$. (b) Vertical profiles of the mean buoyancy fluctuations $\langle B' \rangle$. (c) Vertical profiles of the mean square of the turbulent velocity component $\langle u_z^2 \rangle$. (d) Vertical profiles of the mean square turbulent velocity $\langle u_i^2 \rangle$. The symbol $\langle \cdot \rangle$ denotes an average over $x - y$ planes at fixed z and over a sample of statistically independent turbulence snapshots in all four panels. The line styles are the same for all figures. The horizontal lines in (b), (c) and (d) have been added as a guide to the eye in order to highlight the asymmetry of the profiles.*

flux of moist buoyancy is larger than the flux of dry buoyancy, $\langle u_z M'(z) \rangle > \langle u_z D'(z) \rangle$, and the increase of the buoyancy flux corresponds to the location of the average saturation level. As illustrated in figure 4.3, individual parcels become saturated at different levels so that the buoyancy flux increases gradually with height as the atmospheric layer becomes increasingly saturated. The asymmetry is also manifest in the mean vertical profiles of B' as can be seen in figure 4.6(b). As a further dry reference run, we added data from simulation DRB1a to both panels (see the table). This dry convection run was conducted at the Rayleigh number value Ra_M and we can see that the corresponding profile provides the envelope to the moist data. Panels (c) and (d) show profiles of the velocity fluctuations. Again we can detect asymmetry which is particularly pronounced for the vertical velocity fluctuations. Above the cloud base $z > z_{CB}$, the fluctuations are increased. Slightly stronger vertical updrafts in the saturated part are in line with the enhanced buoyancy flux. However, this enhancement is significantly smaller than the buoyancy flux enhancement.

Figure 4.7 compares the transport properties as a function of the Rayleigh number. We compare the buoyancy flux for runs MRB3 and MRB4. Table 1 showed that the global mean square of velocity fluctuations decreases with increasing Rayleigh number. This is also observed for the vertical mean profiles which are qualitatively similar to those of figure 4.6 (c) and (d), but have a smaller maximum amplitude (not shown). The Reynolds number of the turbulent flow grows with approximately
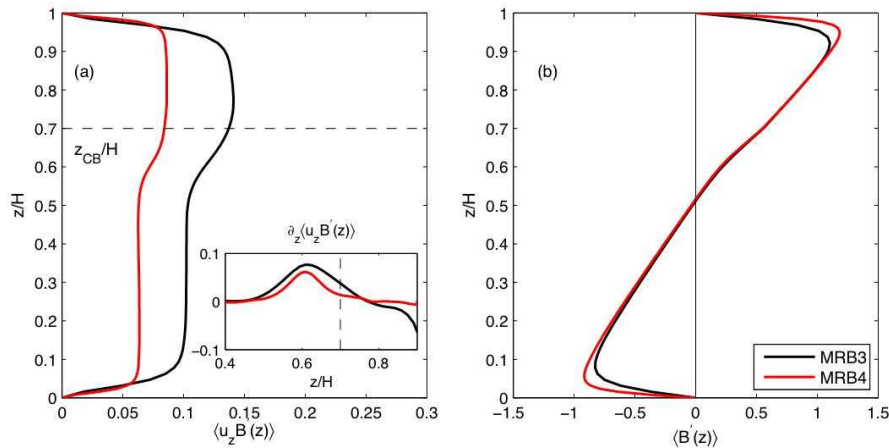
FIG. 4.7. *(a) Vertical profiles of the buoyancy flux $\langle u_z B' \rangle$. The inset displays the local slope of the profile in order to quantify the width of the crossover of the profile. The dashed line indicates the cloud base for both runs. (b) Vertical profiles of the buoyancy fluctuations $\langle B' \rangle$. The average is conducted as in figure 4.6. The line styles are the same for all figures.*

$\sqrt{Ra}$ in turbulent convection. With growing Ra the flow and buoyancy field structures become more filamented since the thickness of the thermal boundary layers at the bottom and top — the main source of coherent thermal plumes in convection — shrinks. This is in line with a smaller mean square amplitude of the velocity. The same trend holds for the buoyancy flux. The profiles for both Rayleigh numbers agree qualitatively, however the amplitudes are smaller and the transition from the unsaturated to the saturated fraction is sharper (see inset of the left panel). The latter property confirms our observations for the cloud base in figure 4.3.

5. Conclusions

Water vapor has a profound impact on atmospheric dynamics through its phase transition and the associated latent heat release. Many atmospheric phenomena from clouds and hurricanes to the planetary-scale circulation can only be fully understood by addressing the role played by phase transition. While significant progress has been made over the last few decades, there remains a need for more theoretical insights on how dynamics and thermodynamics interact in a moist atmosphere. This paper has presented an idealized framework in which the dynamical impacts of phase transitions can be studied while dramatically reducing the complexity of the equation of state.

At the core of our approach lies the fact that a parcel of cloudy air can be treated as being in local thermodynamic equilibrium. In practice, this means that liquid water can only be present if the parcel is saturated. The thermodynamic equilibrium assumption has two important consequences: it reduces the number of state variables necessary to describe the thermodynamic state of moist air to three. The partial derivatives of the equation of state are discontinuous at saturation. Arguably, this discontinuity in the partial derivatives is the key feature of the equation of state that distinguishes moist dynamics from the behavior of a single phase fluid.

To study the dynamic implications of phase transition, we propose an idealized framework that combines a Boussinesq system where buoyancy is a piecewise linear

function of two independent state variables. This framework was initially proposed by [5, 6] but has not been further explored since then. Our approach is to separately linearize the equation of state for saturated and unsaturated parcels. The saturation line, i.e., the boundary between the saturated and unsaturated portion of the state space, must be re-derived to ensure thermodynamic consistency, which in this case boils down to linearizing it. The procedure retains the discontinuity in the partial derivatives along a saturation line, but otherwise simplifies the equation of state such that the buoyancy can be expressed as a piecewise linear function of two prognostic thermodynamic variables.

This framework is used here to study a moist analog to the Rayleigh-Bénard convection. An atmospheric slab is destabilizing by imposing the temperature and water content at both the upper and lower boundaries. It is shown that this problem is characterized by five different dimensionless parameters: two Rayleigh numbers corresponding respectively to the saturated and unsaturated environment, a Prandtl number, a Surface Saturation Deficit (SSD) and the Condensation in Saturated Ascent (CSA). For certain regimes, for example when the slab is fully saturated or fully unsaturated, this problem reduces to the traditional Rayleigh-Bénard convection. However, when the atmospheric slab is partially saturated, new behaviors can emerge such as a conditional instability which occurs when the slab is stable for unsaturated parcels but unstable for saturated parcels. The direct numerical simulations demonstrate the variation of the buoyant flux profiles compared to the dry convection case. Further investigations of the parametric space are under way.

REFERENCES

[1] P.R. Bannon, *On the anelastic approximation for a compressible atmosphere*, J. Atmos. Sci., 23, 3618–3628, 1996.

[2] J. Biello and A.J. Majda, *A new multi-scale model for the Madden-Julian oscillation*, J. Atmos. Sci, 62, 1694–1721, 2005

[3] J. Bjerknes, *Saturated-adiabatic ascent of air through dry-adiabatically descending environment*, Quart. J. Roy. Meteo. Soc., 64, 325–330, 1938.

[4] J. Boussinesq, *Theorie Analytique de la Chaleur, vol. 2.*, Gauthier-Villars, Paris, 1903.

[5] C.S. Bretherton, *A theory for nonprecipitating moist convection between two parallel plates. Part I: thermodynamics and 'linear' solutions*, J. Atmos. Sci., 44, 1809–1827, 1987.

[6] C.S. Bretherton, *A mathematical model of nonprecipitating convection between two parallel plates. Part II: nonlinear theory and cloud organization*, J. Atmos. Sci., 45, 2391–2415, 1988.

[7] D.R. Durran, *Improving the anelastic approximation*, J. Atmos. Sci., 49, 1453–1461, 1989.

[8] K.A. Emanuel, *Atmospheric Convection*, Oxford University Press, 580, 1994.

[9] D.M.W. Frierson, A.J. Majda and O. Pauluis, *Large scale dynamics of precipitation fronts in the tropical atmosphere: a novel relaxation limit*, Commun. Math. Sci., 2, 591–626, 2004.

[10] W. Grabowski, J.I. Yano and M.W. Moncrieff, *Cloud resolving modeling of tropical circulations driven by large-scale SST gradients*, J. Atmos. Sci., 57, 2022–2040, 2000.

[11] I.M. Held, R.S. Hemler and V. Ramaswamy, *Radiative-convective equilibrium with explicit two-dimensional moist convection*, J. Atmos. Sci., 50, 3909–3927, 1993.

[12] H. Johnston and C.R. Doering, *A comparison of turbulent thermal convection between conditions of constant temperature and constant flux*, Phys. Rev. Lett., 102, 064501, 2009.

[13] J.B. Klemp and R.B. Wilhemson, *Simulation of three-dimensional convective storm dynamics*, J. Atmos. Sci., 35, 1070–1110, 1978.

[14] H.L. Kuo, *Convection in a conditionally unstable atmosphere*, Tellus, 13, 441–459, 1961.

[15] H.L. Kuo, *Further studies of the properties of convection in a conditionally unstable atmosphere*, Tellus, 17, 413–433, 1965.

[16] F.B. Lipps and R.S. Hemler, *A scale analysis of deep moist convection and some related numerical calculations*, J. Atmos. Sci., 39, 2192–2210, 1982.

[17] R.A. Madden and P.R. Julian, *Detection of a 40-50 day oscillation in the zonal wind in the tropical Pacific*, J. Atmos. Sci., 28,702–708, 1971.

[18] R.A. Madden and P.R. Julian, *Observations of the 40-50 day tropical oscillation- a review*, Mon. Wea. Rev., 22, 814–837, 1994.

[19] A.J. Majda, *Multiscale models with moisture and systematic strategies for superparameterization*, J. Atmos. Sci., 64, 2726–2734, 2007.

[20] A.J. Majda, *New Multiscale models and self-similarity in tropical convection*, J. Atmos. Sci., 64, 1393–1404, 2007.

[21] A.J. Majda and R. Klein, *Systematic multiscale models for the tropics*, J. Atmos. Sci., 60, 393–408, 2003.

[22] A. Oberbeck, *Über die wärmeleitung der flüssigkeiten bei berücksichtigung der strömungen infolge von temperaturdifferenzen. (On the thermal conduction of liquid taking into account flows due to temperature differences)* , Ann. Phys. Chem., Neue Folge, 7, 271–292, 1879.

[23] Y. Ogura and N.A. Phillips, *Scale analysis of deep and shallow convection in the atmosphere*, J. Atmos. Sci., 19, 173–179, 1962.

[24] G.S. Patterson and S.A. Orszag, *Spectral calculation of isotropic turbulence: efficient removal of aliasing interactions*, Phys. Fluids, 14, 2538–2541, 1971.

[25] O. Pauluis, *Thermodynamic consistency of the anelastic approximation in a moist atmosphere*, J. Atmos. Sci., 65, 2719–2729, 2008.

[26] O. Pauluis and D.M.W. Frierson and A.J. Majda, *Propagation, reflection, and transmission of precipitation fronts in the tropical atmosphere*, Quart. J. Roy. Meteorol. Soc., 134, 913–930, 2008.

[27] D. Randall, S. Krueger, C.S. Bretherton, J.Curry, P. Duynkerke, M. Moncrieff, B. Ryan, D. Starr, M. Miller, W. Rossow, G. Tselioudis and B. Wielicki, *Confronting models with data: the GEWEX cloud systems study*, Bulletin of the American Meteorological Society, 84, 455–469, 2003.

[28] J.R. Saylor and K.R. Sreenivasan, *Differential diffusion in low Reynolds number water jets*, Phys. Fluids, 10, 1135–1146, 2008.

[29] J. Schumacher, *Lagrangian dispersion and heat transport in convective turbulence*, Phys. Rev. Lett., 100, 134502, 2008.

[30] S. Solomon and Dahe Qin and M. Manning and Zhenlin Chen and M. Marquis and K.B. Averyt, *Climate Change 2007 - The Physical Science Basis. Contribution of Working Group I to the Fourth Assessment Report of the Intergovernmental Panel on Climate Change*, M. Tignor and Leroy Miller, Henry (eds.), Cambridge University Press, 996, 2007.

[31] E.A. Spiegel and G. Veronis, *On the Boussinesq approximation for a compressible fluid*, Astrophys. J., 131, 442–447, 1960.

[32] S.N. Stechmann and A.J. Majda, *The structure of precipitation fronts for finite relaxation time*, Theor. Comp. Fluid Dyn., 20, 377–404, 2006.

[33] A Tompkins and G.C. Craig, *Radiative-convective equilibrium in a three-dimensional cloud-ensemble model*, Q. J. R. Meteorol. Soc., 124, 2073–2097, 1998.

[34] R. Verzicco and K.R. Sreenivasan, *A comparison of turbulent thermal convection between conditions of constant temperature and constant heat flux*, J. Fluid Mech., 595, 203–219, 2007.

[35] K.M. Xu and K.A. Emanuel, *Is the tropical atmosphere conditionally unstable?* Mon. Wea. Rev., 117, 1471–1479, 1989.